JOURNAL OF MATERIALS SCIENCE 30 (1995) 1343–1351

Improvement in hydrogen storage characteristics of magnesium by mechanical alloying with nickel

MYOUNG YOUP SONG
Department of Materials Engineering, Chonbuk National University, 664–14 1ga Deogzindong Deogzingu Chonju Chonbuk, 560–756, Republic of Korea

The hydriding and dehydriding kinetics of Mg are reviewed. It is reported that the hydriding and dehydriding reactions of Mg are nucleation-controlled under certain conditions and progress by a mechanism of nucleation and growth, and that the hydriding rates of Mg are controlled by the diffusion of hydrogen through a growing Mg hydride layer.

The hydriding and dehydriding kinetics of Mg can be improved in consequence by a treatment such as mechanical alloying, which can facilitate the nucleation by creating defects and shorten diffusion distances by reducing the effective particle size of Mg.

The hydriding and dehydriding characteristics of mechanically-treated Mg and mechanically-alloyed mixtures with the compositions Mg–x wt % Ni ($x = 5, 10, 25$ and 55) are studied.

The Mg_2Ni phase develops in the mechanically-alloyed mixtures. The Mg–10 wt% Ni and Mg–25 wt % Ni mixtures are activated easily, show much larger hydrogen storage capacities and much higher hydriding rates, and higher dehydriding rates, than other magnesium-based alloys or mixtures.

1. Introduction

Magnesium has many advantages for a hydrogen storage material: large hydrogen storage capacity (7.6 wt%), low cost and abundance in the Earth's crust. But its hydriding and dehydriding kinetics are very slow [1]. Much work to ameliorate the reaction kinetics of magnesium with hydrogen has been effected by alloying certain metals with magnesium [2–9], by mixing metal additives with magnesium [10], by plating nickel on the surface of magnesium [11] and by synthesizing magnesium hydride in the presence of a homogeneous catalyst [12]. In particular, the Mg/Ni–H_2 system has been studied by alloying [3, 13–16] and by plating [11].

Kinetic studies of the hydriding and dehydriding reactions of Mg were carried out by Stander [17, 18]. He reported that the hydriding reaction of Mg is controlled by the diffusion of magnesium interstitials after a rapid surface reaction, and in the dehydriding reaction the movement of the phase boundary is the rate-determining step at hydrogen pressures appreciably different from the equilibrium dissociation pressure. Nucleation seems to play a role at pressures near the equilibrium dissociation pressure.

Another study of the hydriding kinetics of magnesium by Mintz *et al.* [6] claimed that the reaction is controlled by a three-dimensional diffusion of hydrogen through the magnesium hydride product layer.

Karty *et al.* who had investigated hydriding and dehydriding kinetics of Mg in a Mg /Mg_2Cu eutectic alloy [19] reported that the hydriding is rate-limited by the diffusion of hydrogen through a growing Mg hydride layer, and that the dehydriding is rate-limited by the diffusion of hydrogen through a growing Mg layer.

The kinetic study of Isler [20] on the hydriding and dehydriding kinetics of Mg concluded that these reactions proceed by a mechanism of nucleation on the surface and of the growth of these nuclei, and that a continuous layer is then formed by a coalescence of the domains of the Mg hydride or Mg.

Pedersen *et al.* [21] reported that the small particles need a longer time to reach a particular level of reaction ratio than do the bigger particles in the initial hydridation of heat-treated magnesium with different particle sizes (diameter 49–84 μm). Wang *et al.* [9] reported that in their experiment with an alloy $Mg_{0.833}Ni_{0.066}Cu_{0.095}Ml_{0.006}$ the kinetic properties of finer particles (100–149 μm) were even inferior to those of coarser ones (149–420 μm). Douglass [5] reported that there was a nucleation period in the dehydriding reaction of Mg–5 at% Y for the finer particles (88–125 μm) at 623 K after which the rate was linear and slightly less than the release rate of the coarser particles.

As rate-controlling steps for the hydriding and dehydriding reactions of Mg we can consider the following steps: the chemisorption and desorption of H_2, diffusion, phase transformation, gas phase mass transport and nucleation.

This hydriding and dehydriding behaviour of Mg or its alloys according to the particle sizes eliminates the following steps from the rate-controlling step: the chemisorption or desorption of H_2 (since their rates

0022–2461

increase as the surface area is larger), diffusion of hydrogen atoms through the growing hydride layer or through the growing Mg layer (since its rate increases as the diffusion distance gets smaller as the particles get finer), the phase transformation of the solid solution of hydrogen in Mg into Mg hydride or vice versa (since its rate increases as the reaction interface area gets larger as the particles get smaller) and gas phase mass transport of H_2 up to the surface of Mg (the larger the particle, the higher its rates because the larger particles have the larger paths of H_2. However, the particle sizes of the above results are too large to accept that this process controls the reaction. In the case of the Mg_2Ni–H_2 system, of which the reaction is controlled by this process [22, 23], the particle size is about 2 μm).

This suggests that the rate-controlling step of the above results may be nucleation. The smaller the particle sizes, the greater the number of particles per unit quantity of the sample. If the reaction is controlled by nucleation, the longer time is needed for the formation of nuclei in all the particles, the greater the number of particles. The reaction rate will be small, in consequence, as the particles are finer. This suggests that the reactions are controlled by nucleation under the above experimental conditions.

Vigeholm *et al.* [24] studied the hydride formation mechanisms in nearly spherical magnesium powder particles. They concluded that the reaction of magnesium with hydrogen is a nucleation and growth mechanism. They also found that the nucleation is only rate-determining in the initial hydriding, and that the growth is controlled by a fast diffusion of hydrogen from the particle surface along the hydride–metal interface.

All the above works do not agree with one another on the rate-controlling step(s) for hydriding or dehydriding of magnesium. However, there is no contradiction in the points that the hydriding and dehydriding reactions of Mg are nucleation-controlled under certain conditions and progress by a mechanism of nucleation and growth, and that the hydriding rates of Mg are controlled by the diffusion of hydrogen through a growing Mg hydride layer.

The hydriding and dehydriding kinetics of Mg can be improved, by a treatment such as mechanical alloying which can facilitate nucleation by creating many defects on the surface and/or in the interior of Mg, or by the additive acting as active sites for the nucleation and shortening diffusion distances by reducing the effective particle sizes of Mg.

In this work we studied the hydriding and dehydriding characteristics of mechanically-treated Mg and mechanically-alloyed mixtures with the compositions Mg–$x$wt% Ni (x = 5, 10, 25 and 55), and discuss the effects of mechanical alloying and hydriding–dehydriding cycling on the reaction rates of Mg with H_2.

2. Experimental details

For this study magnesium (Alpha) and nickel obtained from nickel carbonyl (3–5 μm particles) were used. The purity of hydrogen employed was 99.9995%. Magnesium and nickel mixtures (about 5 g), with compositions Mg–$x$wt% Ni (x = 5, 10, 25 and 55), were mechanically alloyed under an argon atmosphere in a planetary mill with an acceleration of about 60 ms^{-2} for 5 min. The composition of Mg–55wt% Ni corresponds to that of Mg_2Ni. Hereafter the compositions of the mixtures were expressed by Mg–x% Ni (x = 5, 10, 25 and 55). The planetary mill contained 200 g of stainless steel balls with a diameter of about 4 mm. Magnesium alone (not mixed with nickel) was also treated under the same conditions.

A Sievert's type hydriding apparatus [25] was employed for the measurements of hydriding and dehydriding rates. It consists of a standard volume and a reactor. They are linked to Bourdon gauges which permit measuring the pressure from 0 to 10 bar with a precision of 0.05 bar. The hydrogen pressure was maintained nearly constant during the hydriding reaction by dosing the appropriate quantity of hydrogen from the standard volume to the reactor. During the dehydriding reaction the hydrogen pressure was also maintained nearly constant by sending an appropriate quantity of hydrogen from the reactor to the standard volume. The variation of the hydrogen pressure in the standard volume permits one to calculate the quantity of hydrogen absorbed or desorbed by the sample as a function of time. The amounts of samples used were about 0.44 g for Mg–x% Ni (x = 0, 10, 25 and 55) and about 0.24 g for Mg–5% Ni. X-ray(CuK_α) powder diffraction was used to identify the phases existing in the samples. The microstructures of mixtures after hydriding–dehydriding cycles were observed by scanning electron microscope (SEM).

3. Results

3.1. Development of Mg_2Ni phase according to hydriding–dehydriding cycling

The development of a Mg_2Ni phase according to hydriding–dehydriding cycling was investigated by X-ray diffraction analysis and by measuring the quantities of hydrogen desorbed under a pressure where the Mg hydride (MgH_2) is stable and only the Mg_2Ni hydride (Mg_2NiH_4) decomposes.

Fig. 1 shows X-ray powder diffraction patterns: (a) of the Mg–55% Ni mixture as prepared, (b) of the Mg–10% Ni mixture hydrided at 8 bar H_2, 583 K after 11 hydriding–dehydriding cycles between 0.6 and 8 bar H_2 at 583 K, (c) of the Mg–25% Ni mixture dehydrided under 3.0 bar H_2 at 583 K in the second cycle after being hydrided at 7 bar H_2, 573 K, and (d) of Mg–55% Ni dehydrided after 58 hydriding–dehydriding cycles (during 2 months) between 543 and 583 K, 0 and 8.5 bar H_2. X-ray diffraction (XRD) pattern (a) shows that the Mg–55% Ni as prepared contains metallic Mg and Ni, and that Mg is deformed preferentially along with the (0002) plane. XRD pattern (b) reveals Mg_2NiH_4, MgH_2, Mg and Ni phases with a very small quantity of MgO. This indicates that the Mg_2Ni phase forms with hydriding–dehydriding cycling, and that larger part of Mg is hydrided at 8 bar H_2, 583 K. Under the experimental conditions

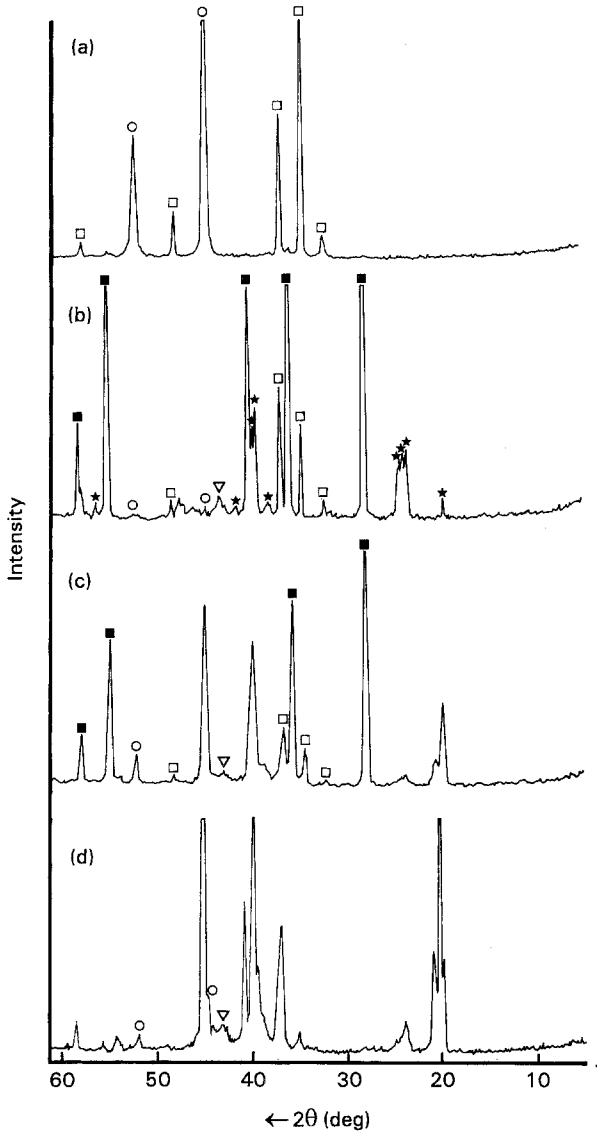

Figure 1 X-ray (CuK_α) powder diffraction patterns of (a) Mg–55% Ni as prepared, (b) Mg–10% Ni hydrided at 583 K, 8 bar H_2 after 11 cycles, (c) Mg–25% Ni dehydrided at 583 K, 3.0 bar H_2 in the second cycle, and (d) Mg–55% Ni dehydrided after 58 cycles at 543–583 K, 0–8.5 bar H_2. □, Mg; ○, Ni; ▽, MgO; ■, MgH_2; ★, Mg_2NiH_4; unmarked, Mg_2Ni.

(3.0 bar H_2, 583 K) of XRD pattern (c) the MgH_2 is stable and only the Mg_2NiH_4 decomposes. XRD pattern (c) shows the Mg_2Ni, MgH_2, Mg and Ni phases with a trace of MgO. On the XRD pattern (d) the peaks characteristic of Mg no longer appear. Small peaks of Ni remain and there is evidence of a small quantity of MgO.

Fig. 2 shows the variation of weight percentages of nickel combined with magnesium under the form of Mg_2Ni [% Ni ($\rightarrow Mg_2Ni$)] in the mechanically-alloyed mixtures as a function of the number of hydriding–dehydriding cycles, n. The percentages of Ni transformed into Mg_2Ni are 1.7 wt% ($n = 19$) for Mg–5% Ni, 9.4 wt% ($n = 10$) for Mg–10% Ni, 22.8 wt% ($n = 10$) for Mg–25% Ni and 40.1 wt% ($n = 17$) for Mg–55% Ni. For these measurements, each mixture was hydrided under 8 bar H_2 at 583 K, and then dehydrided under 2.5 bar H_2 at 583 K for the decomposition of the Mg_2Ni hydride alone.

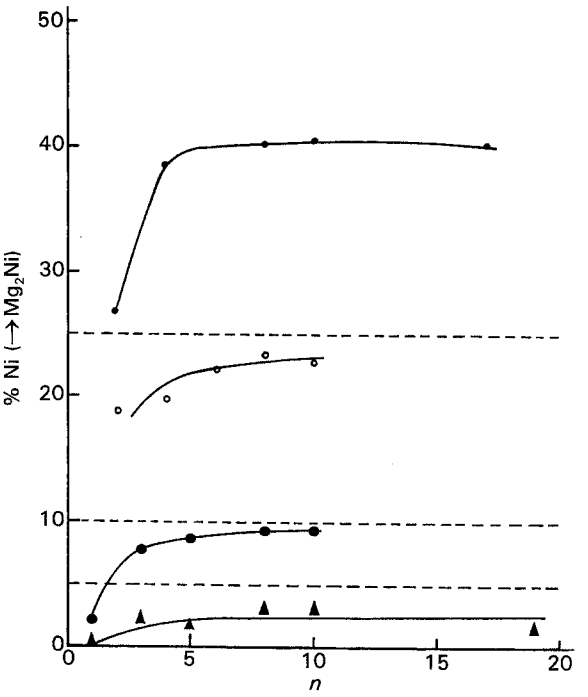

Figure 2 Variation with the number of hydriding–dehydriding cycles n, of wt% nickel transformed into Mg_2Ni [% Ni($\rightarrow Mg_2Ni$)] in the mechanically-alloyed mixtures ●, Mg–55% Ni; ○, Mg–25% Ni; ●, Mg–10% Ni; ▲, Mg–5% Ni.

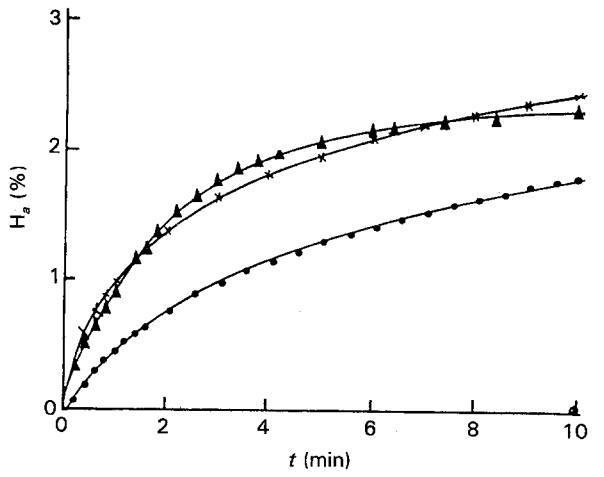

Figure 3 Curves of absorbed hydrogen wt% [H_a(%)] during the first hydriding cycle, at 573 K under 7 bar H_2 as a function of time t. ▲, Mg–55% Ni; ×, Mg–25% Ni; ●, Mg–10% Ni; ⊗, Mg–5% Ni, and Mg.

3.2. Activation process

Fig. 3 gives the curves of weight percentages of hydrogen H_a absorbed during the first cycle of hydriding at 573 K under 7 bar H_2 as a function of time t. The percentages of absorbed hydrogen H_a are expressed with respect to the sample weight. The hydriding rates of Mg–55% Ni and Mg–25% Ni are very similar, and those of Mg–10% Ni are lower. The hydriding rates of Mg and Mg–5% Ni are almost zero. The mechanical treatment of Mg (without Ni) and the mechanical alloying of Mg with 5 wt% Ni under our conditions have little effect on the hydriding rates of the first cycle.

Fig. 4 gives the weight percentages of hydrogen absorbed during 10 minutes [H_a (10 min)] under 8 bar

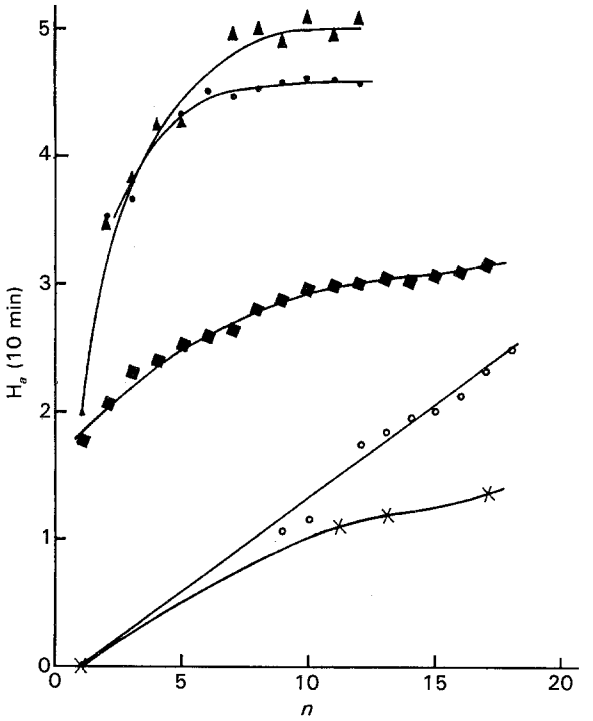

Figure 4 Variation of hydrogen wt% absorbed during 10 min (H_a(10 min)), under 8 bar H_2 at 583 K, as a function of the number of hydriding cycles n. ▲, Mg–10% Ni; ●, Mg–25% Ni; ◆, Mg–55% Ni; O, Mg–5% Ni; ×, Mg.

H_2 at 583 K as a function of the number of hydriding–dehydriding cycles n. At $n = 2$, Mg–25% Ni has the largest H_a (10 min) value. The H_a (10 min) values of Mg–10% Ni, Mg–25% Ni and Mg–55% Ni mixtures are 4.99, 4.52 and 2.78 for $n = 8$. The H_a (10 min) values of Mg–5% Ni and Mg (without Ni) attain only to 2.32 and 1.36 even for $n = 17$. The Mg–10% Ni shows a remarkable increase in H_a (10 min) value between $n = 1$ and $n = 8$.

3.3. Hydriding reaction

Fig. 5 shows the variation of absorbed hydrogen weight percent H_a as a function of time t for each sample at 583 K under 8 bar H_2 and at the n-th hydriding cycle. In the beginning of the reaction, the hydriding rate dH_a/dt (% min^{-1}) of Mg–10% Ni is highest, followed in order by those of Mg–25% Ni, Mg – 5% Ni and Mg–55% Ni. However, the quantities of hydrogen absorbed after two minutes decrease in the order Mg–10% Ni, Mg–25% Ni, Mg–55% Ni and Mg–5% Ni. Mg (without Ni) shows the lowest hydriding rate.

3.4. Dehydriding reaction

Fig. 6 shows the variation of the desorbed hydrogen weight percentage H_d for each sample as a function of time t at 583 K under 1.5 bar H_2 and at the n-th dehydriding cycle. The percentage of desorbed hydrogen H_d is expressed with respect to the sample weight. The quantities of the hydrogen absorbed before dehydriding are indicated between parentheses. The hydrided Mg–55% Ni mixture desorbs about 85% of the absorbed hydrogen in five minutes. Among the other mixtures, the hydrided Mg–25% Ni desorbs hydrogen most rapidly. It is followed in order by Mg–10% Ni

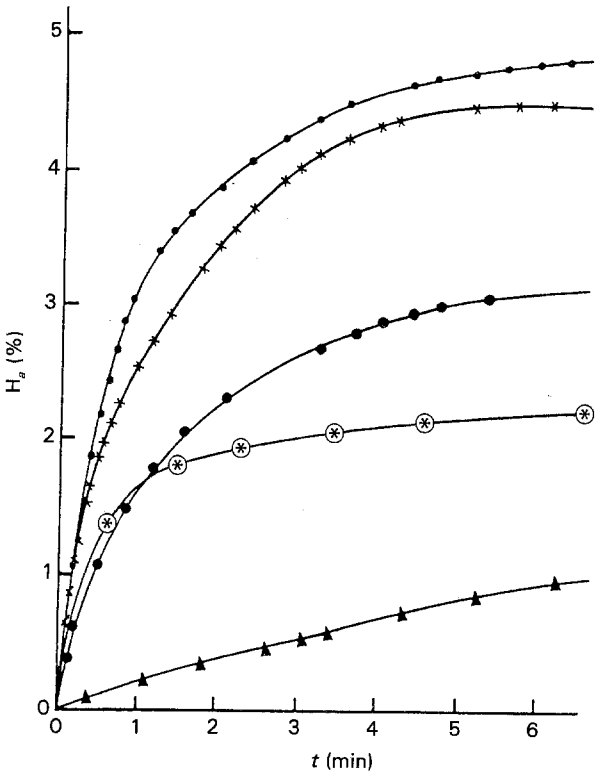

Figure 5 Curves of absorbed hydrogen wt% (H_a(%)) as a function of time t, at the n-th hydriding cycle at 583 K under 8 bar H_2. ●, Mg–10% Ni ($n = 11$); ×, Mg–25% Ni ($n = 11$); ●, Mg–55% Ni ($n = 17$); ⊛, Mg–5% Ni ($n = 17$); ▲, Mg ($n = 17$).

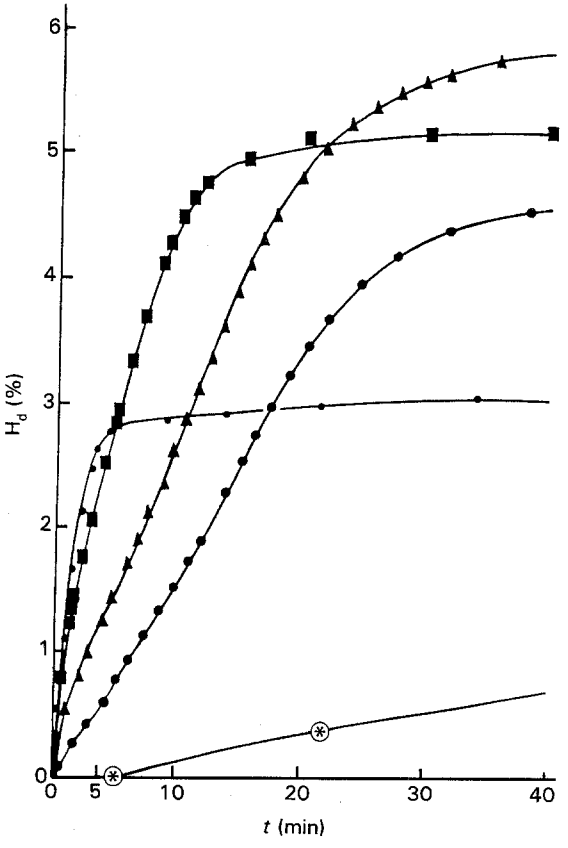

Figure 6 Curves of desorbed hydrogen wt% (H_d(%)) as a function of time t, at the n-th hydriding cycle at 583 K under 1.5 bar H_2. ■, Mg–25% Ni ($n = 11$, 5.32% H); ▲, Mg–10% Ni ($n = 11$, 6.19% H); ●, Mg–5% Ni ($n = 17$, 4.68% H); ●, Mg–55% Ni ($n = 16$, 3.22% H); ⊛, Mg ($n = 16$, H > 4.18%).

and Mg–5% Ni. Mg (without Ni) desorbs hydrogen very slowly after the latency period of about five minutes. The curves for Mg–55% Ni, Mg–25% Ni, Mg–10% Ni and Mg–5% Ni mixtures show two stages. It is considered that the Mg_2Ni hydride decomposes mainly in the first stage, having higher dehydriding rates than the Mg hydride, of these dehydriding curves [26].

3.5. Microstructures before and after hydriding–dehydriding cycling

The topographies and the chemical maps are given in Fig. 7 for the cross-sections of Mg–5% Ni and Mg–55% Ni before hydriding. Fig. 7a for Mg–5% Ni shows that Mg is deformed preferentially along with one plane, which is proved to be the (0 0 0 2) plane by X-ray diffraction analysis. The chemical maps by back-scattered electrons (Fig. 7b and d) show the distributions of nickel. Nickel is represented as white points on the chemical maps. The Mg–55% Ni mixture is formed with strata of magnesium and nickel (Fig. 7c and d).

Fig 8 shows the microstructures of Mg–10% Ni before and after hydriding–dehydriding cycling; (a), (b) and (d) are their chemical maps and (c) is its topography.

4. Discussion

The hydrogen storage properties of the mechanically-alloyed Mg–x% Ni (x = 0, 5, 10, 25 and 55) mixtures

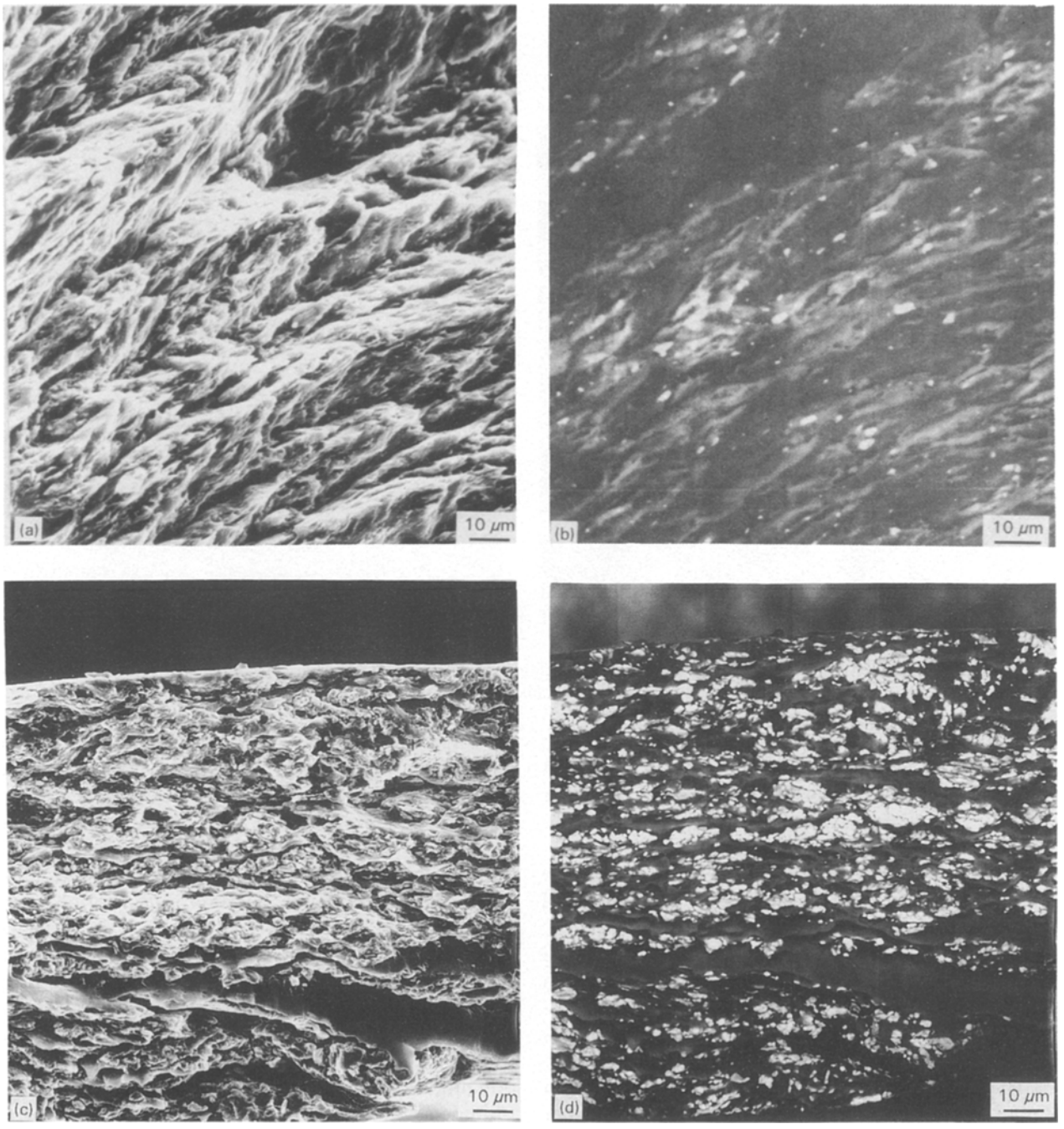

Figure 7 Microstructures observed by SEM for the cross-sections of Mg–5% Ni and Mg–55% Ni as prepared. (a) Mg–5% Ni, topography; (b) Mg–5% Ni, distribution of nickel; (c) Mg–55% Ni, topography; (d) Mg–55% Ni, distribution of nickel.

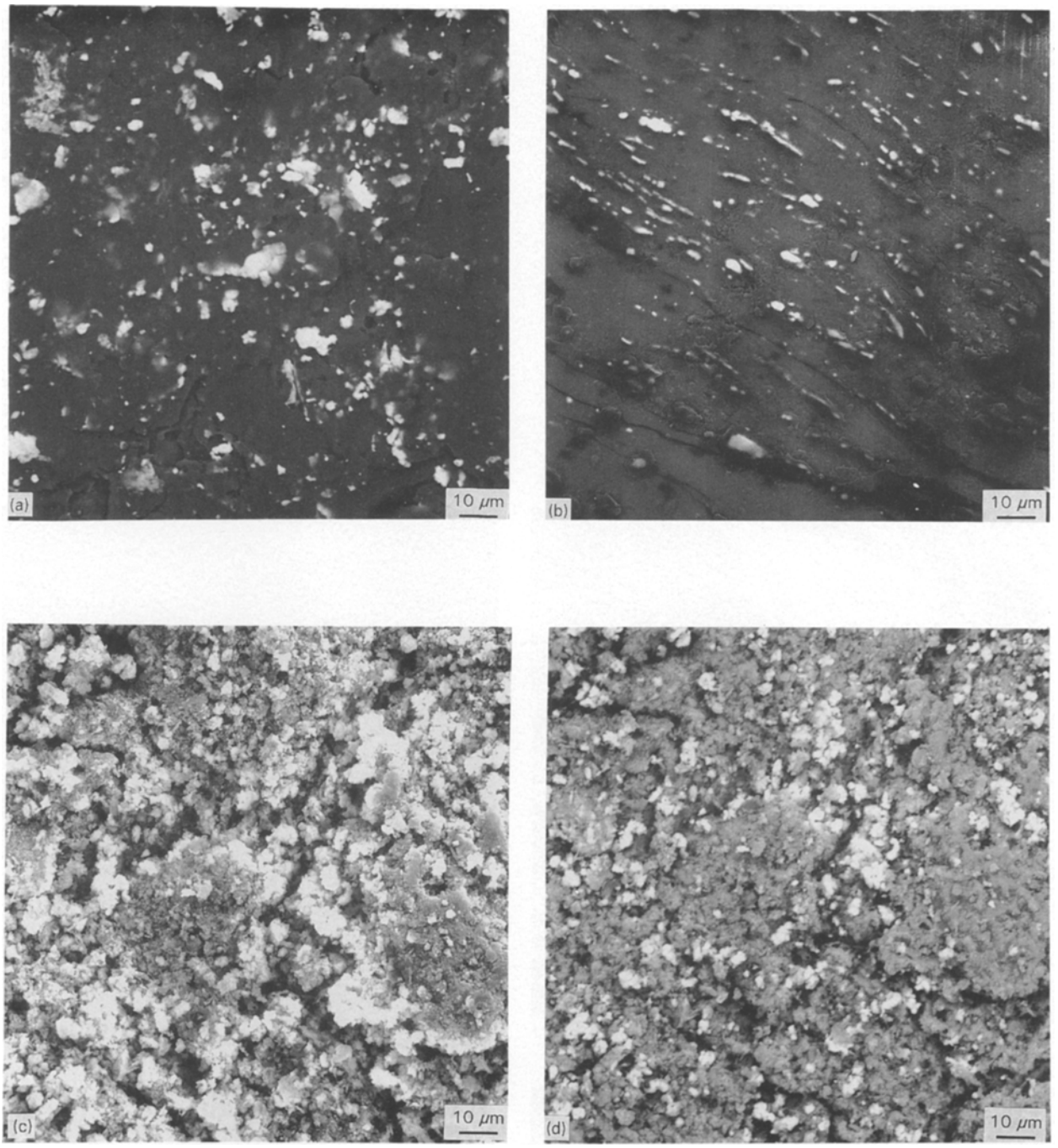

Figure 8 Microstructures observed by SEM of Mg–10% Ni before and after hydriding cycling. (a) Distribution of nickel, $n = 0$; (b) distribution of nickel (cross-section), $n = 0$; (c) topography, $n = 7$; (d) distribution of nickel, $n = 7$.

are summarized in Table I. The numbers are the orders of the mechanically-alloyed mixtures for each hydrogen storage property. The smaller number indicates the higher value of hydrogen storage property.

In Table I, were compared for the hydrogen storage capacities of the samples, the weight percentages of hydrogen absorbed during 1 h at 8 bar H_2 583 K.

This table shows that Mg–10% Ni and Mg–25% Ni are the most favourable compositions for hydrogen storage. The Mg–10% Ni and Mg – 25% Ni absorbed hydrogen of 6.19 wt% (for 18.4 h), 5.32 wt% (for 13.5 h), respectively, for $n = 11$ at 583 K, 8 bar H_2.

The Mg–10% Ni and Mg–25% Ni showed much larger hydrogen storage capacities and much higher hydriding rates, and higher dehydriding rates, than other magnesium-based alloys or mixtures [26].

Fig. 9 shows the variation of reacted fraction F after 1 h under 7 bar H_2 at 573 K as a function of the number of hydriding–dehydriding cycles n. The reacted fraction F is defined as the ratio of the mole number of hydrogen absorbed during time t to the mole number of hydrogen calculated on the assumption that 100% of the mixture is transformed into Mg_2NiH_4 or MgH_2. Curve A concerns the mechanically-alloyed Mg–55% Ni and curve B the Mg_2Ni alloy prepared by fusion. From the first hydriding cycle the mechanically-alloyed Mg–55% Ni mixture attains $F = 0.64$ ($H_a = 2.39$ wt%) whereas that of the Mg_2Ni alloy is only 0.49 ($H_a = 1.83$ wt %). The activation of the mechanically-alloyed Mg–55% Ni mixture is achieved after about ten hydriding–dehydriding cycles and that of the Mg_2Ni alloy after about 15 cycles. However, the hydrogen storage capacity of the

TABLE I Hydrogen storage properties of the mechanically-alloyed mixtures (The smaller number means the better hydrogen storage property)

Properties \ Composition	Mg	Mg–5% Ni	Mg–10% Ni	Mg–25% Ni	Mg–55% Ni
dH_a/dt at $n = 1$	4	4	3	1	1
H_a(10 min) at $n = 8$	5	4	1	2	3
dH_a/dt	5	3	1	2	4
dH_d/dt	5	4	3	2	1
Hydrogen storage capacity	5	4	1	2	3
Total	24	19	9	9	12
Rating	5	4	1	1	3

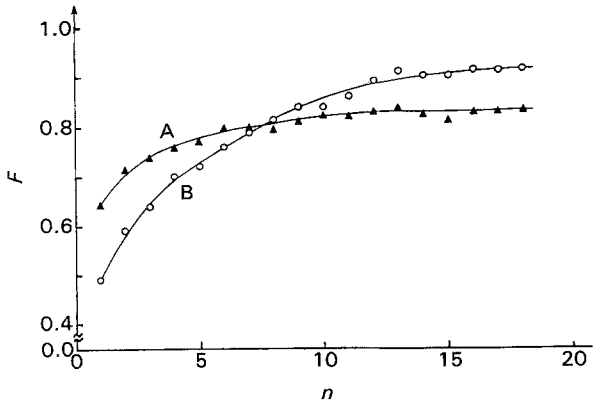

Figure 9. Variation of reacted fraction F after 1 h at 573 K, 7 bar H_2 as a function of the number of cycles n for the Mg–55% Ni mixture (curve A) and for the Mg_2Ni alloy (curve B).

mechanically-alloyed Mg–55% Ni mixture is smaller than that of the Mg_2Ni alloy.

Fig. 10a shows the variation of the hydriding rates dF/dt of a Mg_2Ni alloy with reduced time $t/t_{0.5}$ ($t_{0.5}$ corresponds to the time when F is 0.5) at 563 K under different hydrogen pressures. Under 6 and 6.5 bar H_2, the initial trend of the nucleation and growth mechanism does not appear, while under pressures equal to and lower than 5.5 bar H_2 it does appear. This is considered to result from the slow nucleation of the Mg_2Ni hydride under such relatively low pressures. Fig. 10b shows the variation of dF/dt of a mechanically-alloyed Mg–55% Ni (corresponding to the composition Mg_2Ni) with $t/t_{0.5}$ at 563 K. In this mixture, about 40.1 wt% Ni (among 55 wt% Ni) is transformed into Mg_2Ni and the rest of the nickel (about 14.9 wt%) remains metallic. The magnesium which did not combine with nickel stays metallic. The hydriding rate of Mg is lower than that of Mg_2Ni. Under only 4.5 and 4 bar H_2 the initial trend of the nucleation and growth mechanism appears.

Under 5 and 5.5 bar H_2 the Mg_2Ni alloy shows the initial trend of the nucleation and growth mechanism while the mechanically-alloyed Mg–55% Ni does not, even though the latter contains Mg having a lower hydriding rate. This fact suggests that the nucleation of hydride is more favourable in the mechanically-alloyed mixture than that in the alloy.

Mechanical treatment or mechanical alloying by planetary mill is considered to enlarge specific surface area and augment the number of defects on the surface

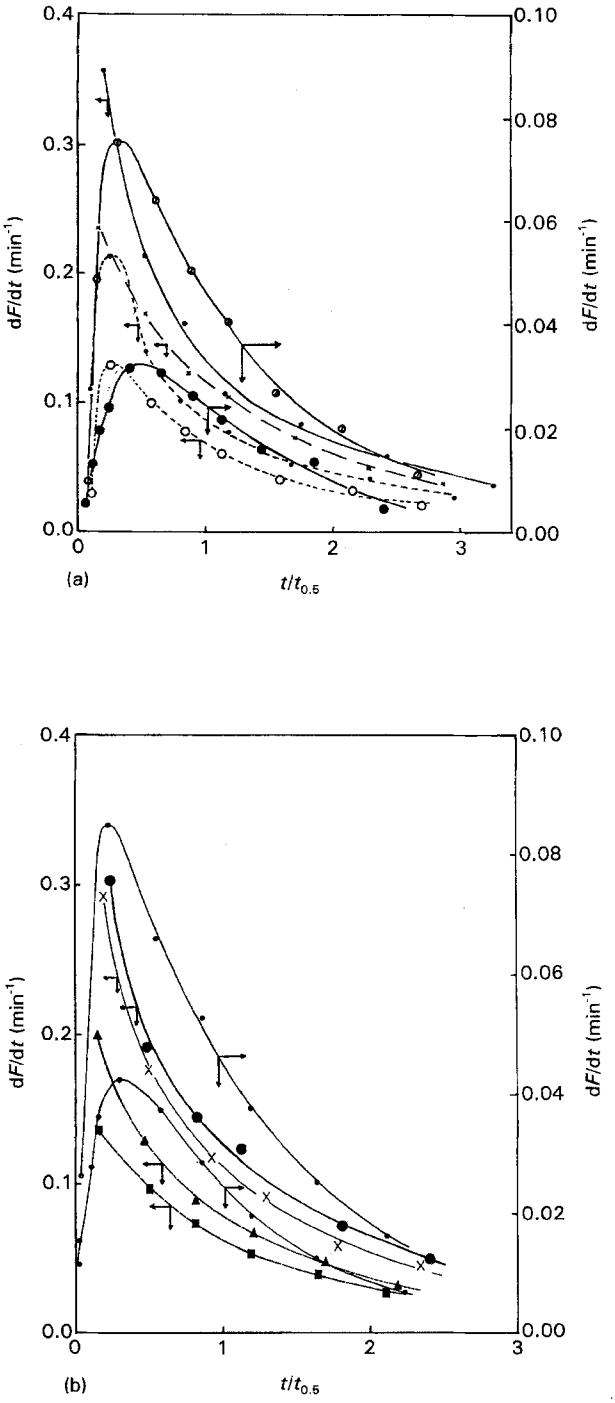

Figure 10. Variation of hydriding rates dF/dt with reduced time $t/t_{0.5}$ at 563 K under different hydrogen pressures of (a) the Mg_2Ni alloy (●, 6.5 bar; X, 6 bar; ○, 5.5 bar; ○, 5 bar, ⊘, 4.5 bar; ●, 4 bar) and (b) the Mg–55% Ni mixture (●, 6.5 bar; X, 6 bar; ▲, 5.5 bar; ■, 5 bar; ○, 4.5 bar; ●, 4 bar).

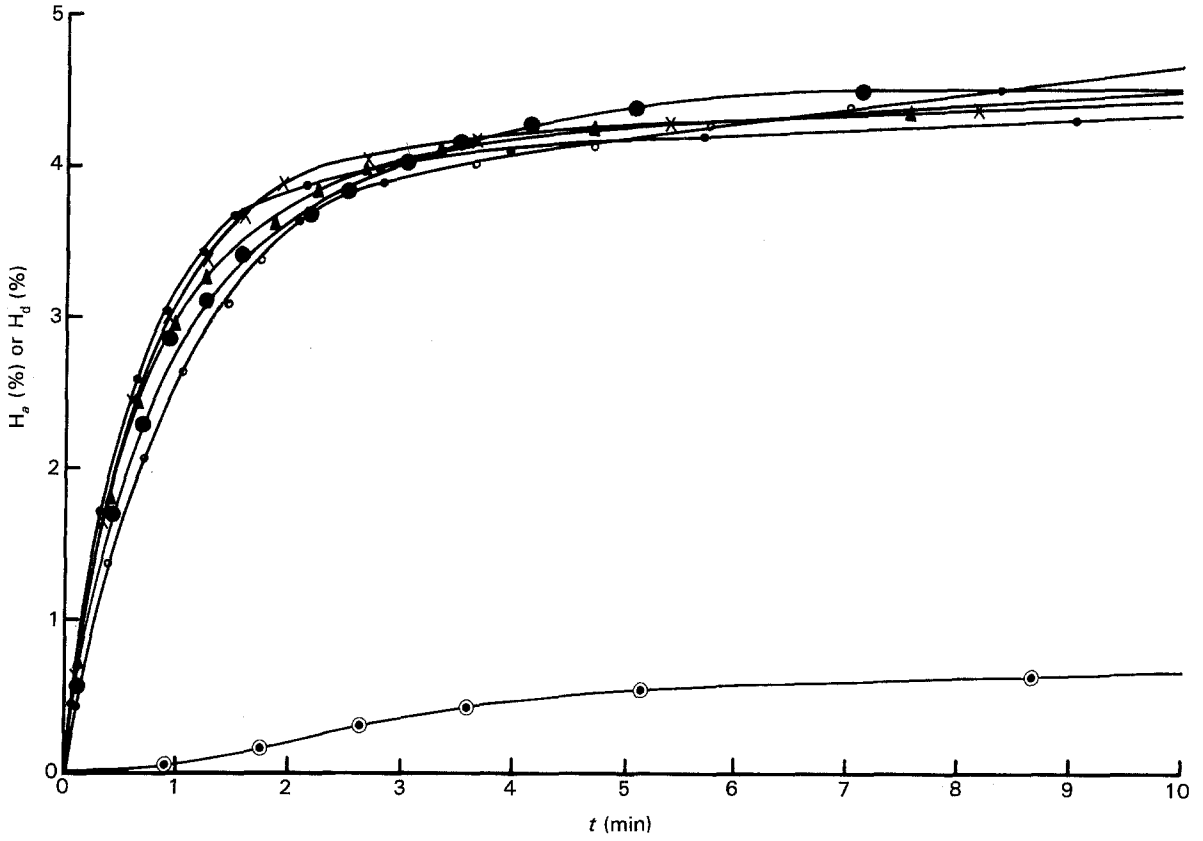

Figure 11 Hydriding curves of Mg–10% Ni under 7 bar H_2 at 543–583 K (●, 543 K; X, 553 K; ▲, 563 K; ●, 573 K; ○, 583 K) and a dehydriding curve under 2.5 bar H_2 at 583 K (⊙).

as well as in the interior of the materials. The expansion and contraction of the lattice during hydriding–dehydriding cycling favours the diminution of particle size and can create numerous defects. On the contrary the annealing effect during hydriding–dehydriding cycling can bring about diminution of specific surface area by sintering and decrease in the number of defects.

The defects created on the surface and in the interior and/or Ni and Mg_2Ni (or Mg_2Ni hydride) formed during hydriding–dehydriding cycling, in the mechanically-alloyed mixtures, can be nucleation sites for the Mg_2Ni hydride and/or the Mg hydride. This is considered to facilitate the nucleation of hydride in the mechanically-alloyed mixtures.

Fig. 11 gives the curves of weight percentages of hydrogen H_a absorbed in the Mg–10% Ni mixture as a function of time t under 7 bar H_2 at temperatures between 543 and 583 K. A dehydriding curve is also given under 2.5 bar H_2 at 583 K. Under this condition only the Mg_2Ni hydride decomposes. This dehydriding curve shows that the Mg_2Ni absorbs hydrogen – about 0.75 wt% of the sample. Since Mg_2Ni hydride is formed more rapidly than Mg hydride, the formation of Mg_2Ni hydride is considered to be completed at the beginning of the reaction. The hydriding rates of Mg_2Ni depend inversely on temperature in this temperature range [22]. The hydriding curves of Fig. 11 show an inverse dependence on temperature up to $H_a \simeq 3.5$ wt%, and then they show a normal temperature dependence. The hydriding rates of Mg were reviewed in the above to be controlled by diffusion which shows a normal temperature dependence, through a growing Mg hydride layer. These results suggest that diffusion is not a rate-controlling step up to $H_a \simeq 3.5$ wt% in the hydriding reaction of Mg–10% Ni.

Therefore it is considered that the mechanical alloying has changed the rate-controlling step (up to $H_a \simeq 3.5$ wt%) in the hydriding reaction of Mg from diffusion into another step.

A detailed study on the hydriding kinetics of a mechanically-alloyed mixture Mg–10 wt% Ni [27] showed that the rate-controlling step of hydriding reaction is the gas phase mass transport of H_2 and the chemisorption of H_2 up to $H_a \simeq 4.25$ wt%, after which the diffusion of hydrogen through the growing hydriding layer controls the reaction. The augmentation of surface area (in consequence, the decrease in effective particle sizes) by the effects of the mechanical alloying and hydriding–dehydriding cycling, changed the rate controlling step of hydriding reaction of Mg (up to $H_a \simeq 4.25$ wt%) from diffusion into these steps. The kinetics study on the dehydriding reaction of a mechanically-alloyed mixture Mg–10 wt% Ni [27] showed that intrinsic processes are not rate-controlling steps from the beginning of the dehydriding reaction up to $H_a \simeq 4.5$ wt%, where the dehydriding reaction is controlled by the gas phase mass transport of H_2. This step is expected to be a possible rate-controlling one when the particles are small and/or porous. The effects of mechanical alloying and hydriding–dehydriding cycling decreased the effective particle sizes and made the material porous (Fig. 8c and d).

5. Conclusions

The hydriding and dehydriding kinetics Mg are reviewed. The hydriding and dehydriding reactions of Mg are nucleation-controlled under certain conditions and progress by a mechanism of nucleation and growth, and the hydriding rates of Mg are controlled by the diffusion of hydrogen through a growing Mg hydride layer.

Therefore, in order to improve the hydriding and dehydriding kinetics of Mg, the nucleation must be facilitated by creating many defects and the diffusion distances of hydrogen shortened by reducing the effective particle size of Mg. For these purposes, Mg was alloyed mechanically with nickel.

The hydrogen storage properties of the mechanically-treated Mg and the mechanically-alloyed Mg–x wt% Ni (x = 5, 10, 25 and 55) mixtures have been investigated.

The Mg_2Ni phase develops in the mechanically-alloyed mixtures along with hydriding–dehydriding cycling. In view of activation, hydriding and dehydriding rates and hydrogen storage capacity, Mg–10 wt% Ni and Mg–25 wt% Ni are the most favourable compositions.

The Mg–10 wt% Ni and Mg–25 wt% Ni absorbed hydrogen of 6.19 wt% (for 18.4 h), 5.32 wt% (for 13.5 h), respectively, for n = 11 at 583 K, 8 bar H_2.

The Mg–10 wt% Ni and Mg–25 wt% Ni showed much larger hydrogen storage capacities and much higher hydriding rates, and higher dehydriding rates, than other magnesium-based alloys or mixtures.

The defects created on the surface and in the interior of the material and/or Ni and Mg_2Ni (or Mg_2Ni hydride) formed during hydriding–dehydriding cycling are considered to facilitate the nucleation of hydride in the Mg–55 wt% Ni as compared with that in the Mg_2Ni alloy.

The augmentation of surface area by mechanical alloying and hydriding–dehydriding cycling has changed the rate-controlling steps of the hydriding and dehydriding reactions of Mg–10 wt% Ni into the gas phase mass transport of H_2.

Acknowledgement

This is a part of the work supported financially by Yonam Foundation (Korea) for visiting research abroad in 1992.

References

1. A. VOSE, "Metal Hydrides", U.S. Patent 2 944 (1961) p. 587.
2. J. J. REILLY and R. H. WISWALL, *Inorg. Chem.* **6**(12) (1967) 2220.
3. J. J. REILLY and R. H. WISWALL Jr, *Inorg. Chem.* 7(11) (1968) 2254.
4. D. L. DOUGLASS, *Metall. Trans. A*, **6** (1975) 2179.
5. D. L. DOUGLASS, in A. F. Anderson and A. J. Maeland (eds.), "Hydrides for Energy Storage", Proceedings International Symposium Geilo, Norway, August 1977, pp. 151–184.
6. M. H. MINTZ, Z. GAVRA and Z. HADARI, *J. Inorg. Nucl. Chem.* **40** (1978) 765.
7. M. PEZAT, A. HBIKA, B. DARRIET and P. HAGENMULLER, French Anvar Patent 78 203 82, 1978. *Mater. Res. Bull.* **14** (1979) 377.
8. M. PEZAT, B. DARRIET and P. HAGENMULLER, *J. Less-Common Met.* **74** (1980) 427.
9. Q. WANG, J. WU, M. AU and L. ZHANG, in "Hydrogen Energy Progress V", Proceedings 5th World Hydrogen Energy Conference, Toronto, Canada, July 1984. Vol. 3, edited by T. N. Veziroğlu and J. B. Taylor (Pergamon, New York) pp. 1279–1290.
10. B. TANGUY, J. L. SOUBEYROUX, M. PEZAT, J. PORTIER and P. HAGENMULLER, *Mater. Res. Bull* **11** (1976) 1441.
11. F. G. EISENBERG, D. A. ZAGNOLI and J. J. SHERIDAN III, *J. Less-Common Met.* **74** (1980) 323.
12. B. BOGDANOVIC, *Int. J. Hydrogen Energy*, **9**(11) (1984) 937.
13. E. AKIBA, K. NOMURA, S. ONO and S. SUDA, *Int. J. Hydrogen Energy*, 7(10) (1982) 787.
14. E. AKIBA, K. NOMURA and S. ONO, *J. Less-Common Met.* **89** (1983) 145.
15. J. M. BOULET and N. GERARD, *J. Less-Common Met.* **89** (1983) 151.
16. S. ONO, Y. ISHIDO, E. AKIBA, K. JINDO, Y. SAWADA, I. KITAGAWA and T. KAKUTANI, in "Hydrogen Energy Progress V", Proceedings 5th World Hydrogen Energy Conference, Toronto, Canada, July 1984, Vol. 3, edited by T. N. Veziroglu and J. B. Taylor (Pergamon, New York) pp. 1291–1302.
17. C. M. STANDER, *Z. Physik Chem.* **104** (1977) 229.
18. C. M. STANDER, *J. Inorg. Nucl. Chem.* **39** (1977) 221.
19. A. KARTY, J. GRUNZWEIG-GENOSSAR and P. S. RUDMAN, *J. Appl. Phys.* **50**(11) (1979) 7200.
20. J. ISLER, Thèse de 3ème cycle, Université de Dijon (France), 1979.
21. A. S. PEDERSON, J. KJOLLER, B. LARSEN and B. VIGEHOLM, in "Hydrogen Energy Progress V", Proceedings 5th World Hydrogen Energy Conference, Toronto, Canada, July 1984, Vol. 3, edited by T. N. Veziroğlu and J. B. Taylor, (Pergamon, New York) pp. 1269–1277.
22. M. Y. SONG, M. PEZAT, B. DARRIET, J. Y. LEE and P. HAGENMULLER, *J. Mater. Sci.* **21** (1986) 346.
23. M. Y. SONG, B. DARRIET, M. PEZAT, J. Y. LEE and P. HAGENMULLER, *J. Less-Common Met.* **118** (1896) 235.
24. B. VIGEHOLM, K. JENSEN, B. LARSEN and A. SCHRODER PEDERSEN, *J. Less-Common Met.* **131** (1987) 133.
25. M. Y. SONG, M. PEZAT, B. DARRIET and P. HAGENMULLER, *J. Solid State Chem.* **56** (1985) 191.
26. M. Y. SONG, E. IVANOV, B. DARRIET, M. PEZAT and P. HAGENMULLER, *J. Less-Common Met.* **131** (1987) 71.
27. M. Y. SONG, (in press)

Received 23 September 1993
and accepted 28 June 1994